

RESEARCH ARTICLE

Optimized Design of a Wireless Charger Prototype for an e-Scooter

**ALICIA TRIVIÑO-CABRERA^{ID}, JUAN C. QUIRÓS^{ID}, JOSE M. GONZÁLEZ-GONZÁLEZ^{ID},
AND JOSÉ A. AGUADO^{ID}, (Member, IEEE)**

Department of Electrical Engineering, University of Málaga, 29010 Málaga, Spain

Corresponding author: Alicia Triviño-Cabrera (atc@uma.es)

This work was supported in part by Spanish Ministerio de Ciencia e Innovación (MICINN) through the “Proyectos de Research, Development and innovation (I+D+i)—RTI Tipo A” Programme under Project PID2019-110531-RA-I00/AEI/10.13039/501100011033.

ABSTRACT Individual mobility vehicles are revolutionizing transportation in the urban environment. Among them, e-scooters are one of the fastest growing vehicles. However, these vehicles have some drawbacks such as incompatibility among different chargers or reduced autonomy, which especially affects e-scooters rental. Wireless charging is presented as a solution to these drawbacks since it allows the batteries to be charged without user intervention. This paper addresses the design process and implementation details related to a magnetic-resonance charger for an e-scooter. In contrast to the previous works, we present a comprehensive approach that addresses the design of the coil topology, the dimensions of the ferrite tiles, the definition of the gap and the optimised control for a CC-CV charge. The main contribution of the work is the consideration of all these issues jointly while we also take into account the vehicle’s materials and structure for an accurate design and implementation. The dimensions of the vehicle impose a strong restriction on the coil design. Therefore, a detailed analysis about the location of the secondary and primary coils in a real e-scooter is executed with Ansys Maxwell. The study about the geometries of ferrite tiles is also performed considering the particularities of this type of vehicle. This study led to an optimal solution for the coil geometries and ferrite placement that minimizes the costs. The proposed system has been validated with the implementation of a real prototype of 100 W, to which a CC-CV control has been incorporated to achieve a safe charge for different battery states. The control can be easily adapted for a wide range of e-scooters. In this way, the use of this type of chargers on public installations can be maximized.

INDEX TERMS Wireless power transfer, coil design, e-scooter, ferrite layout, CC-CV control, magnetic field.

I. INTRODUCTION

The United States Environmental Protection Agency and the European Union state that light vehicles are causing a relevant contribution to the greenhouse gas emissions (nearly 20% of the total) [1]. In order to reduce this effect, governments are favouring Electric Vehicles (EVs) with specific regulatory policy and economic incentives. There are multiple types of EVs and their suitability depends on the number of passengers, journey distances, type of routes, etc. The number of electric scooters, bicycles and motorcycles has increased in

recent years as they represent a comfortable solution for personal mobility in cities, especially in those cities that suffer from high congestion rates. Due to this problem, last-mile mobility based on EVs is becoming a fundamental piece in urban management [2]. It is expected that the congestion rates will be greater in the future, according to the Coordinates Institute for Governance and Applied Economics, 60% of the world population will reside in large cities by 2050. In this context, strategies that promote personal mobility transport, such as electric scooters, are being developed. These vehicles, both owned and temporarily rented, have significant advantages such as low cost, reduced energy consumption, easy parking and practicality [3]. In addition, the use of e-scooters

The associate editor coordinating the review of this manuscript and approving it for publication was Amin Mahmoudi^{ID}.

in urban routes increasingly fosters complementing the travels with other means of public transport (metro, bus, train, etc.), which further reduces the use of private vehicles [4].

Nowadays, most of the scooters batteries are based on lithium-ion technology [5]. For its charging, conductive charging is mainly used, which are provided with different connectors. According to [6], the main disadvantages in order to own an EV, like an e-scooter, are the battery price, the vehicle autonomy and the minimal charging infrastructure in the urban environment. This last limitation restricts the procedure followed by some companies that operate renting e-scooters. Multiple cities already have agreements with companies so that they can offer their electric scooters for rent for a short period of time. The charging process is currently carried out with an inefficient process that reduces the availability of EVs. An operator collects the scooters and transfers them to a specific charging point where there are multiple chargers. Once recharged, an operator must carry out the reverse operation by placing them in the EV “parking lots”. Proceeding in this way is mainly motivated by the risks that plug-in unattended platforms will represent as they could be accessed without any precaution by non-expert people. Users with their own electric scooter also find that there are no grid connection sockets easily available in the urban environment. As described by the report on micromobility prepared by EIT InnoEnergy [7], it is recommended to adopt a systemic and sustainable approach to improve the platforms for charging personal vehicles.

It is evident that electric scooters can benefit from advanced chargers integrated in cities. These chargers must enable safe, controlled and autonomous recharging. Wireless chargers are highlighted as one of the potential solutions for personal mobility transport [8], which provides a safe charging while it avoids dealing with different grid connectors [9]. In this paper, we present a wireless charger for an e-scooter. Wireless Power Transfer (WPT) is already being used in other EVs [10]. These chargers avoid the existence of electrical connections to the electrical network that could cause health problems for users due to improper operation. The wireless connection could also reduce the fraudulent use of these facilities, even without an operator supervision. Wireless chargers are mainly based on resonant inductive WPT techniques. Unlike the conductive charger that operates at 50 Hz, the wireless charger must increase the operating frequency to achieve the levels required by the EV battery. To do this, both the charging platform and the wireless charger in the EV consist of power converters, filters and capacitors, in addition to a pair or air-coupled coils. The efficiency of the power transfer is related to the coupling coefficient of the coils. Since the power range required by the e-scooters is lower than 1 kW, their wireless chargers could be easily integrated into current power systems with minimal infrastructural modifications. This capability enables the strategic deployment of the chargers for high utilization.

Inductive WPT chargers, in some specific electric cars, are already available in the market, so we can conclude that they

have reached a mature status [11]. However, a limited number of experiments have been conducted so far with other types of vehicles such as e-scooters. As can be observed in Table 1, some previous works have addressed a preliminary design of inductive wireless chargers for e-scooters. However, the proposed designs have not fully considering the materials and effects of the scooter. Moreover, they were not implemented on a real and functional vehicle [12], [13], [14], [15], [16]. Since magnetic field is modified with metallic objects, design and implementations without the real e-scooter may not derive realistic conclusions. In addition, it is necessary to charge the e-scooter batteries conveniently with a Constant Current-Constant Voltage (CC-CV) method in order to prolong their lifetime. This type of control has only been implemented in [16] but without an optimization to achieve maximum efficiency in the power transfer. As for the frequency of the magnetic field, references [12], [13] opted for 6.78 MHz whereas [14], [15], [16] based their design on 200, 400 and 150 kHz frequencies, respectively. Concerning the operational frequency, previous works do not comply with SAE J2954 [11], which is the standard for wireless chargers for light-duty EVs. Series-Series (SS) compensation is the usual reactive network in these works.

The comprehensive application of WPT to e-scooters, including optimal coil design and enhanced control, is not straightforward, as it has been demonstrated by some previous designs of wireless chargers for e-bicycles [17] or wheelchairs [9]. The particular position of the surrounding materials, the location of the battery and the temperature of the vehicle are key elements that affect the WPT. In addition, weight and physical stability are critical in an e-scooter. These two conditions may not be fulfilled with the incorporation of bulky and heavy electronic components for the power receiver. The power receiver must also be economic, to be a convenient solution for these low cost EVs. The same criteria must be the basis for the CC-CV control that these batteries require.

Considering these premises, we have proceeded with a complete design of a wireless charger for an e-scooter. The design takes into account the materials and structure of the e-scooter. The coil design is based on a realistic model of the vehicle using a Finite Element Analysis (FEA) tool. Then, the complete design is used for the implementation of the charger in a real e-scooter, where some valid conclusions are derived. In addition, a CC-CV control has been included to charge the e-scooters appropriately for different battery states. The control adapts the configuration of a DC/DC converter to achieve maximum efficiency during the whole charging process. In the previous works (as summarized in Table 1), we cannot find the implementation of all these features altogether.

The main contributions of this work are:

- The design of the wireless charger is carefully performed to consider the physical stability, the weight restrictions and minimal costs imposed by conventional scooters while achieving an appropriate efficiency in the WPT.

TABLE 1. Previous implementations of e-scooters chargers.

Reference	Frequency	Compensation	Coils	Vehicle effect in design	Vehicle effect in implementation	CC-CV charging	MEPT
[13]	6.78 MHz	SS	Square		✓		
[12]	6.78 MHz	SS	Circular				
[14]	200 kHz	SS	Mixed		✓		
[15]	400 kHz	SS	Square				
[16]	[140-200 kHz]	SS	Square			✓	
Our proposal	85 kHz	SS	Circular	✓	✓	✓	✓

These criteria impact on the determination of the coils' dimensions and the size of the ferromagnetic materials.

- As summarized in Table 1, this is the first contribution to the related literature where a precise design of a wireless charger is validated with a real scooter. The characterization of the coupled coils with an FEA software is also carried out considering a model which includes the dimensions and materials of this type of vehicle.
- The working frequency is adapted to the SAE J2954 standard [11]. Once this standard is widely deployed, we believe that components for wireless chargers complying with SAE J2954 are expected to be cheaper and it will probably decrease the costs associated with the implementation proposed. For this frequency range, the WPT coils are made of litz wires to reduce losses due to skin effect. The material is accurately modelled in the FEA tool.
- A CC-CV control is incorporated to the charger to guarantee a safe charge for the different battery states associated with a complete charge. The control configures the secondary DC/DC converter and the input voltage according to a Maximum Efficiency Point Tracking (MEPT) algorithm. The control operates on the secondary side, and it sends information to the primary side in order to set the input voltage that gives maximum efficiency. The DC/DC converter can be easily adapted to different battery models. In this way, the primary circuit is valid for a wide range of e-scooter models.

The remainder of the paper is structured as follows. Section II describes the coil design, which prioritizes maximizing the coupling coefficient. Based on the coil design, Section III explains how the compensation topology was selected. Section IV shows the implementation on a real e-scooter and includes some experimental results (electrical, thermal and magnetic measurements). Finally, Section V concludes the paper.

II. DESIGN OF THE COUPLED COILS

In our approach, we intend to have a realistic performance of the coils once it is installed on the e-scooter. Thus, for the coil design, Ansys Maxwell software is used [18]. This FEA software lets us include the structure and materials of the e-scooter so that their effect on the WPT can be accurately modelled. A 3D model was developed for this purpose. This model represents a generic e-scooter and can be seen in Figure 1. However, the model is too complex for FEA analysis

**FIGURE 1.** 3D e-scooter model.

due to multiple details and pieces which does not affect significantly. A simpler model is developed in this work to reduce computational costs and provide realistic results. The final model is composed of the basic structure of the e-scooter without the parts whose size is insignificant compared to the structure or are far from the coils. Other components whose materials do not interfere with magnetic fields, such as tires, are also not included.

The main goal of the coil design is to select the ideal pair of coils which maximizes the coupling coefficient while minimizing their cost. The position of the coils on the scooter is the first decision to be taken. Multiple positions could be suitable for this component. This decision is affected by three main constraints: the available space, which is limited in an e-scooter, the interference with the user, and the surrounding materials, which affects the magnetic field and the power transfer. The bottom of the scooter is the selected position because interference with the user is almost non-existent and the primary coil can be located on the ground without any additional structure. Multiple authors also consider this position as the most convenient option [12], [13], [15], [16].

As commented, geometrical constraints must be taken into account for the design. These constraints are presented in Figure 3. Considering these space limitations, multiple options for the coil sizes are analyzed. Misalignment is not considered in the analysis since we assume that the parking of the e-scooter is fixed by a structure that ensures the correct position of the receiving coil. Figure 2 shows a representative



FIGURE 2. Generic e-scooter parking lot [19].

parking lot for e-scooters where this condition can be guaranteed.

The topology of the coils affects their complexity and costs. The lower the complexity, the lower the cost. Some complex geometries are proposed in the related literature for wireless chargers when some factors (such as misalignment) are present [20]. However, these particularities are not present in our application and simple coil geometries provide a similar performance than complex and more expensive coils. Thus, we only considered simple coil geometries. The simplest coil geometries are the circular and the rectangular ones [21]. In [22] the authors conclude that for aligned positions, circular coils give higher coupling coefficient than rectangular ones. Following this analysis, circular coils are considered for our design. Taking into account the space restrictions, multiple options for circular coils are possible. We have evaluated which one is the best in the particular application of an e-scooter. For this operation, FEA simulations have been done with the potential solutions of circular coils and the adapted 3D-model for the e-scooter.

The design of this charger is partially based on the SAE J2954 standard. One of the main requirements of this standard is the operating frequency, which is established at 85 kHz with a tolerance margin. This frequency requires the use of a special type of cable (litz wire) for the coils to minimize losses due to the skin effect. FEA simulations with litz wire are time-consuming since their multiple strands make computational cost increase. To model the coils in Ansys Maxwell, an homogenization process will be executed. The homogenization process consists in simplifying the litz wire as an equivalent layer with the same electrical properties [23]. This process allows reducing computational costs while improving simulation times. Multiple options are possible considering the space constraint of the e-scooter base. It is important to note that a wide set of simulations has been performed to find the optimal design that meets the requirements so reducing the computational time provides a notable advantage to the design.

Due to the effect of the scooter on the magnetic field, the secondary coil requires as much space as possible in order to maximize the coupling coefficient between the primary and secondary coils. For a litz wire of 200 strands of AWG-38,

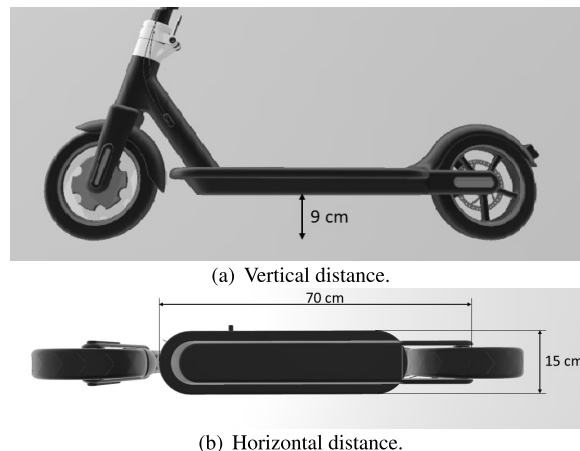


FIGURE 3. Geometrical restrictions.

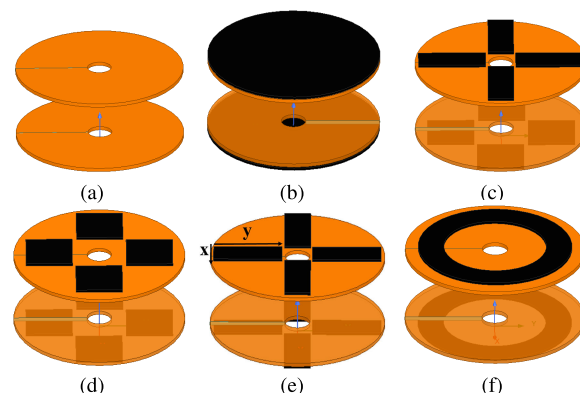


FIGURE 4. Different layouts for ferrite tiles. a) Without, b) Completed, c) Radial mixed tiles, d) Radial wide tile, e) Radial thin tile, e) Ring.

the selected coil has 20 turns with an inner radius of 1 cm. The diameter of the litz wire is 3 mm.

In order to choose the optimal combination of coils, the primary coil is configured with the same geometry than the secondary coil. Its final configuration is decided analyzing the effects of the ferrite layouts and different number of turns (from 20 to 50 turns). These two issues will be explained next.

A. FERRITE LAYOUT

Ferromagnetic materials are sensitive to external magnetic fields as their inner ions easily orientate in the same direction than the external field. This property makes them a suitable option to improve wireless power transmission. The distribution of ferrite tiles is important in terms of effectiveness-cost. The works in [24] and [25] show that radial positions have high relation amount of ferrite-effectiveness for in-wheel applications and electric cars respectively. In contrast to our application, the coils in these previous works are larger so we have evaluated this assumption for our specific case. For an e-scooter, the layout of the ferrite tiles in the coils is crucial in order to optimize the amount of material used for the power transfer, the costs and weight. Different layouts can be considered as shown in Figure 4.

In Table 2 the coupling coefficient for the different layouts can be seen. For a simplicity purpose, we consider that the

TABLE 2. Parameters for different ferrite layouts.

Layout	$L_1(\mu H)$	$L_2(\mu H)$	K	Area (mm^2)
Figure 4 (a)	25.235	25.246	0.156	0
Figure 4 (b)	41.219	41.233	0.196	15393
Figure 4 (c)	31.579	33.635	0.174	5405
Figure 4 (d)	31.572	31.565	0.172	5776
Figure 4 (e)	33.513	33.499	0.176	5035
Figure 4 (f)	28.619	28.734	0.166	6283

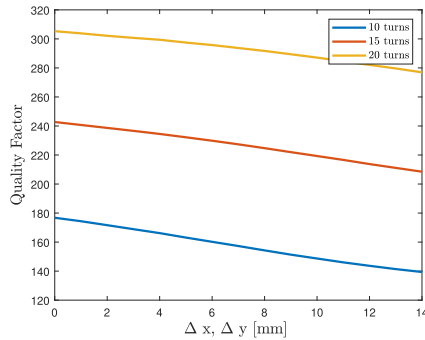


FIGURE 5. Quality factor versus the modification of the size of the ferrite tiles.

primary and the secondary coils have the same dimensions. The simulations carried out with Ansys Maxwell show that radial layouts (Figures 4 c, d and e) are capable of increasing the coupling coefficient with less material used, thus being these the most efficient in order to reduce the amount of material, costs and weight. Layouts like those in Figure 4b achieve maximum coupling coefficient although it needs a great amount of material, which increases the costs and weight of the charger.

One of the main drawbacks of including ferrite tiles could be the extra weight added by ferrite tiles in the secondary coil. However, it is insignificant (few grams) compared to the weight of the vehicle (around 12 kg) and the user’s weight (around 70 kg). The layout with radial positions (Figures 4.c, d and e) provide a good weight, cost and performance ratio. To further analyse the radial layouts, we will consider other parameters affecting the WPT. First, we will study how the size of the ferrite tiles impacts on the quality factors of the coils. Figure 5 illustrates the evolution of the quality factor with the variations of height and width for different number of turns. For a generic ferrite tile with width x and height y , as depicted in Figure 4.e, we increase the width by Δx and decrease the height by Δy . We assume that $\Delta x = \Delta y$. The variation in Figure 5 forces moving from rectangular tiles to square tiles. As expected, for higher number of turns the quality factor of the coil is higher than for smaller ones. An important conclusion from these results is that the variation of quality factor is not so relevant for lower number of turns: for 20 turns of the coil, the reduction is 9.29 %, but for a 10-turn coil the reduction is 21.15 %. These results show that rectangular tiles are more suitable for smaller coils but some additional analysis could be done for larger coils as the variation of the quality factors is not so severe. This study will be done next once the dimensions of the primary coil are determined.

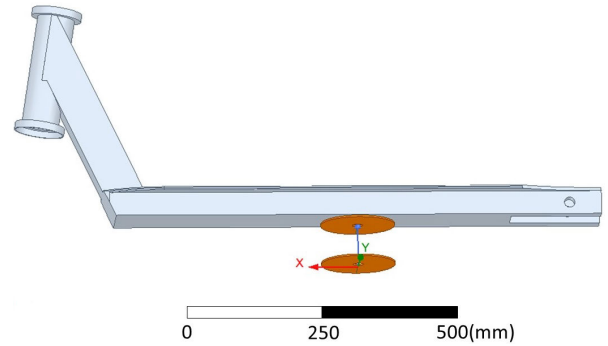


FIGURE 6. Coil simulation in Ansys Maxwell.

B. DIMENSIONS OF THE PRIMARY COIL

The decision about the number of turns to build the primary coil is based on an iterative process in which the coupling coefficient and the costs are analysed. Thus, for each potential design solution (number of turns) of the primary coil, we have studied four compositions of the coils: (i) no ferrite included, (ii) ferrite incorporated only on the primary coil, (iii) ferrite added exclusively on the secondary coil and (iv) ferrite tiles are installed on both the primary and secondary coils. The ferrite tiles are incorporated with a radial layout using wide tiles for the primary coil and thin tiles for the secondary coil (see Figure 4c). The study is performed with Ansys Maxwell, being the model of the coils depicted in Figure 6.

The distance between the primary and the secondary coil is another constraint. Most scooters have a vertical distance between the ground and the base of 9 cm approximated so this distance will be considered as a starting point for our analysis. The simulations are initially performed with this air gap for the four types of configurations. Results in Figure 7 show a maximum coupling coefficient of 0.1139 with a 35-turn primary coil with ferrite tiles in both coils. This coupling coefficient can be considered low for this application because typical coupling coefficients are between 0.1 and 0.3 [26] and the value is very close to the lower side of the range.

In order to improve the coupling coefficient while reducing the costs, the air gap between the primary and the secondary coil was reduced to 6.5 cm. With this configuration, we assume that the parking lot could be equipped with a higher platform where the primary coil is embedded. This is a feasible assumption considering that typical parking lots have the structure to keep the e-scooter in vertical positions and the front wheel static. The results for this new configuration are presented in Figure 7. As can be observed, the maximum coupling coefficient was 0.199 with a 28-turn primary coil. The result shows that with an air gap reduction, we are also able to reduce the necessary number of turns of the primary coil and, therefore, its cost and weight. This reduction helps saving around 4.66 m of litz wire.

In order to select the final coil configuration, we have to attend two main requirements: coupling coefficient and costs. Although the maximum value is reached for 28 turns with a coupling coefficient of 0.199, the final solution was adopted for a 25 turns coil as it has a similar coupling. The coupling

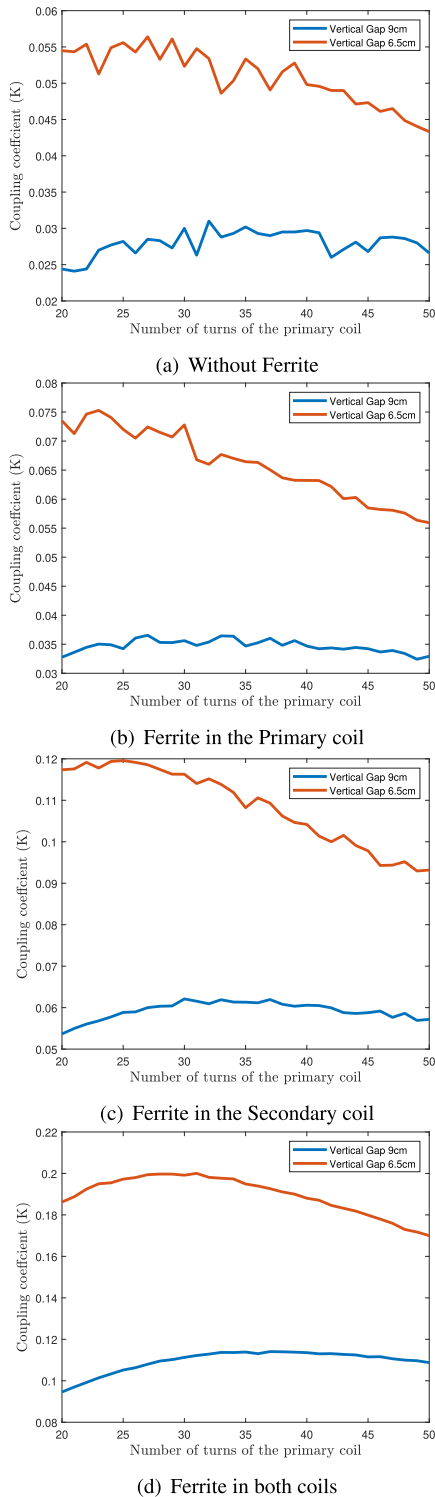


FIGURE 7. Coupling coefficient with different configuration of the primary coils and gaps.

coefficient with this configuration is 0.197, which is very close to the optimal value. The difference on the coupling is almost insignificant but we achieve to further reduce the amount of wire needed in 1.71 m.

Finally, a comparative between thin and wide ferrite tiles in the primary coil has been performed. Previously, in Figure 5

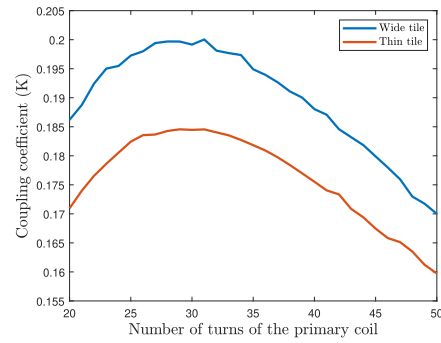


FIGURE 8. Comparative of the performance with wide and thin ferrite tiles in the primary coil.

TABLE 3. Design parameters of the developed coils.

Primary coil		Secondary coil	
L_1	63.5747 μH	L_2	24.6846 μH
$r_{1, in}$	1 cm	$r_{2, in}$	1 cm
$r_{1, out}$	8.5 cm	$r_{2, out}$	7 cm
N_1	25	N_2	20
M		7.8145 μH	

it was proved that square ferrite tiles may be suitable for coils that have higher number of turns. In Figure 8 the variation of the coupling coefficient with the number of turns of the primary coil can be seen for wide and thin ferrite tiles (with dimensions depicted in Figure 4. d and e, respectively). Results show that wide tiles in the primary coil achieve higher coupling coefficient than thin tiles. As we demonstrated previously, when the number of turns of the primary coil is significant, the variation of the coupling coefficient is not relevant (please refer to Figure 5). Thus, we will opt for the cheapest and lightest version of the wide tiles which provides an acceptable quality factor, that is, for square tiles.

The final ferrite layout will be square tiles in the primary coil and rectangular tiles in the secondary coil. The size of the ferrite tiles in the primary coil are $55 \times 55 \text{ mm}^2$ while on the secondary side, the dimensions are $65 \times 23 \text{ mm}^2$. The final amount of litz wire used for this prototype is 12.9 m (7.70 m for the primary coil and 5.2 m for the secondary coil). It can be observed that the steps carried out during the design for the reduction of the litz wire have a significant contribution with 4.66 m with the selection of the gap and 1.71 m with the definition of the number of turns for the primary coil.

The theoretical electrical characteristics of the circular coils for the selected configuration are summarized in Table 3, where r_x, in and r_x, out represent the inner radius and outer radius respectively for $x = 1$ if the primary coil is considered and $x = 2$ for the secondary coil. The outer radius depends directly of the number of turns (N_x). The relation between between M and k is determined by $M = K \sqrt{L_1 L_2}$.

III. COMPENSATION SYSTEMS

One of the main requirements for e-scooter wireless charger is to minimize the complexity and costs. There is a wide variety of e-scooters and their batteries have different electrical features. There are some working at 42 V and others at 36 V.

TABLE 4. Compensation capacitors value for different compensation networks.

Compensation	C_1	C_2
SS	$\frac{1}{L_1 \omega^2}$	$\frac{1}{L_2 \omega^2}$
SP	$\frac{L_2^2 C_2}{L_1 L_2 - M^2}$	$\frac{1}{L_2 \omega^2}$
PS	$\frac{L_2 C_2}{L_1 + \frac{M^4}{L_1 L_2 C_2 R_L^2}}$	$\frac{1}{L_2 \omega^2}$
PP	$\frac{(L_1 L_2 - M^2) L_2^2 C_2}{M^4 R_L^2 C_2 (L_1 L_2 - M^2)^2}$	$\frac{1}{L_2 \omega^2}$

To ease the deployment of wireless chargers, the primary circuit must be valid for all these types of batteries. Consequently, we consider that including a voltage adaptation on the secondary side is the most convenient approach.

With this premise, the most simple structure of an EV wireless charger is depicted in Figure 9. As for the power converters, only a rectifier and an inverter are included on the primary side. The secondary side has a non-controllable rectifier and a DC/DC converter to adapt the voltage levels to the requirement of the battery of the e-scooter on which it is installed. It is desirable that the specific voltage level required by the battery can be configured with a software tool.

Regarding the compensation networks, uni-resonant topologies offer a cost-effective solution, specially suitable for wireless charging with null or not relevant coil misalignments [16], [17]. This is the type of scenarios we are working with the e-scooter, so we will study these compensation networks.

Uni-resonant topologies can be classified in four categories, depending if capacitors are installed in series or parallel. These topologies, illustrated in Figure 10, are Series-Series (SS), Series-Parallel (SP), Parallel-Series (PS) and Parallel-Parallel (PP). Our design process consists of evaluating the potential configurations of the system with these four topologies. In these schematics, the output inverter V_1 is a sinusoidal wave assuming a first harmonic approximation. The impedance of the battery at the input of the secondary rectifier is modelled as the resistance R_L (referred to as the equivalent load resistance). The relation between the internal resistance of the battery R_{Bat} and R_L depends on the configuration of the secondary DC/DC converter, as it will be explained in Section IV.

With the parameters of the designed coils, the electrical performance of each compensation topology can be studied. The procedure to compute the capacitors is different depending on the compensation topology. Table 4 summarizes the equations of these elements, where ω corresponds to the operational angular frequency. Complying with SAE J-2954 requirements, we are working with an operational frequency of 85 kHz.

The efficiency, the voltage and current on the primary side (\vec{V}_1 and \vec{I}_1) can be computed according to Table 5. In [21], the authors present a complete description about how to derive these equations.

For our design, the requirements of the charger include a charging power of 100 W and a secondary voltage of 40 V.

Uni-resonant topologies have been analyzed considering these requirements and using Equations in Table 5. PP and PS compensations need high voltage and low current to charge at 100 W. SS and SP compensations use lower voltages so they will be considered due to this levels of voltage are more reachable and safer. Table 6 shows that SS and SP compensations use almost the same levels of current and voltage with a constant resistance on the secondary side. The SS compensation is selected because of its easier design and implementation.

IV. PROPOSED CC-CV CONTROL

Lithium-ion batteries need to be charged with a specific method in order to extend their durability. This method consists of a two-phase charging process known as CC-CV. This method proceeds with charging at constant current until the maximum voltage recommended by the manufacturer is reached. The chosen current in this stage depends on the power requirements of the battery. Using current levels under the maximum one helps to increase the lifespan. In the second phase of the charging process, the voltage level is regulated to keep this parameter constant. In this second process, the current starts decreasing until the battery is completely charged.

In this paper we propose the use of a complete CC-CV charge in the wireless charging process. The control is only installed on the secondary side and it does not require any parameter/measurement from the primary side. The secondary side informs about the convenient setting of the primary side to work at maximum efficiency while providing the appropriate voltage to the battery. In this way, the primary circuit is simple and useful for different types of e-scooters. When installing the charger on the e-scooter, the control must be configured to update the reference values according to the battery features. Figure 11 shows a theoretical CC-CV charging application for a battery of an e-scooter. It has a first constant-current stage at 2.5 A in which the voltage increases, followed by a constant-voltage stage at 40 V in which the charging current gradually decreases. These voltage and current levels are typical for e-scooter batteries. It can be seen that during the charging process the equivalent resistance of the battery changes as a nonlinear function.

For our proposal, the CC-CV control technique is implemented using a single PI controller, as depicted in Figure 12. This PI controller regulates both current and voltage chargings simultaneously. A PI input error selector makes this possible, preventing both voltage and current from exceeding the limit values of the battery. The main advantages of this solution are its simplicity of implementation and a seamless transition from CC to CV.

The control works as follows. First, the voltage (V_m) and current (I_m) on the battery are measured. These measurements will not be sent via a wireless connection because the control is only placed on the secondary side. Then a selector chooses the charging mode depending on the voltage value. If this level is under the maximum recommended by the manufacturer, the charging mode will be constant current and if this

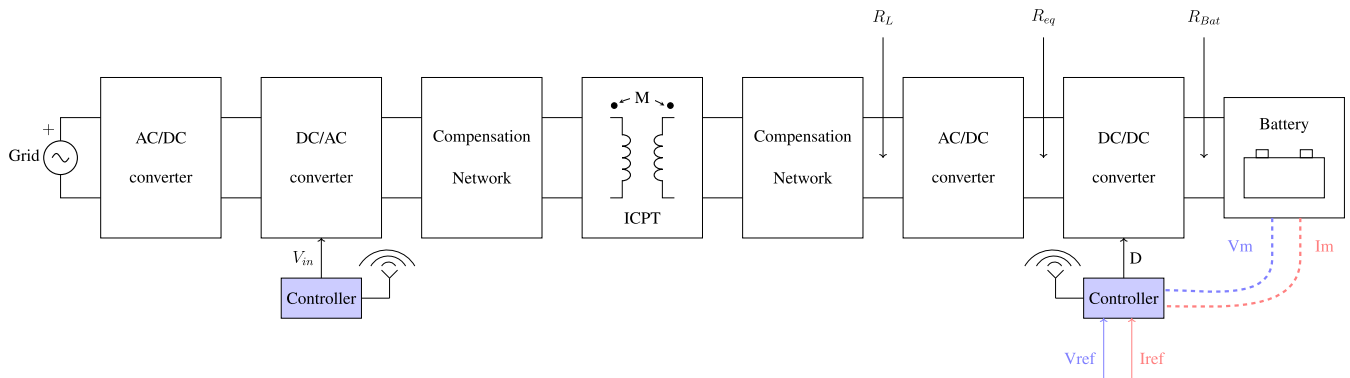


FIGURE 9. Structure of the proposed charger topology.

TABLE 5. Voltage, current and efficiency for different compensations.

Comp	\vec{V}_1	\vec{I}_1	η
SS	$(R_1 + j\omega L_1 + \frac{1}{j\omega C_1}) \vec{I}_1 - j\omega M \vec{I}_2$	$\frac{[(R_2 + R_L) + j(L_2\omega - \frac{1}{C_2\omega})] \vec{I}_2}{j\omega M}$	$\frac{R_L}{R_1 (\frac{R_2 + R_L}{\omega M})^2 + R_2 + R_L}$
SP	$(R_1 + j\omega L_1 + \frac{1}{j\omega C_1}) \vec{I}_1 - j\omega M \vec{I}_2$	$\frac{[R_L + (R_2 + jL_2\omega)(1 + jR_L C_2\omega)] \vec{I}_2}{j\omega M}$	$\frac{R_L}{R_L + R_2 + \frac{R_2 R_L^2}{\omega^2 L_2^2} + \frac{R_1 R_2^2}{\omega^2 M^2}}$
PS	$(R_1 + j\omega L_1) \vec{I}_1 - j\omega M \vec{I}_2$	$\frac{[(R_2 + R_L) + j(L_2\omega - \frac{1}{C_2\omega})] \vec{I}_2}{j\omega M} + j\omega C_1 \vec{V}_1$	$\frac{R_L}{(R_L + R_2)(1 + R_1 \frac{R_2 + R_L}{\omega^2 M^2})}$
PP	$(R_1 + j\omega L_1) \vec{I}_1 - j\omega M \vec{I}_2$	$\frac{[R_L + (R_2 + jL_2\omega)(1 + jR_L C_2\omega)] \vec{I}_2}{j\omega M} + j\omega C_1 \vec{V}_1$	$\frac{R_L}{R_L + R_2 + \frac{R_1 L_2}{M^2} + \frac{R_2 R_L^2}{\omega^2 L_2} + \frac{R_1 R_2^2}{\omega^2 M^2}}$

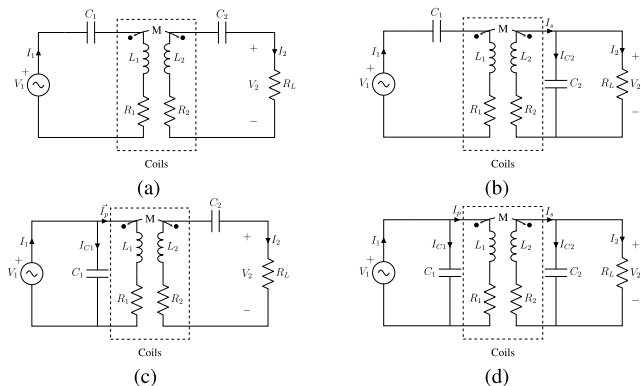


FIGURE 10. Uni-resonant compensation topologies: (a) Series-Series, (b) Series-Parallel, (c) Parallel-Series, (d) Parallel-Parallel.

TABLE 6. Required voltage and current with uni-resonant compensation networks.

Compensation topology	V_1	I_1	V_2	I_2
SS	12.42 V	8.68 A	40 V	2.78 A
SP	12.31 V	8.82 A		
PS	294.85 V	0.37 A		
PP	288.14 V	0.51 A		

value is equal or higher, the charging mode will be constant voltage. V_{ref} corresponds to the maximum indicated by the battery manufacturer, which is configured in the controller via software. It is important to highlight the fact that compatibility with other e-scooter models is ensured as the charging

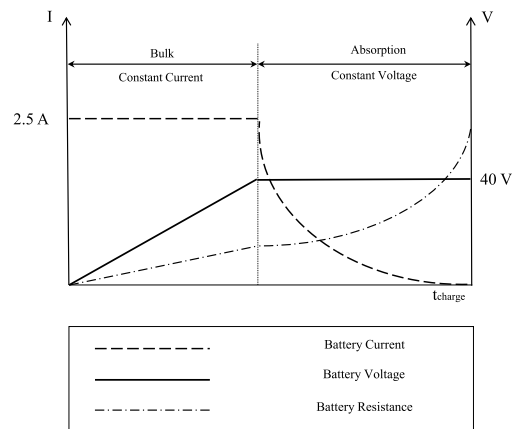


FIGURE 11. CC-CV charge.

references and the selector's decision are based on the battery parameters.

To comply with the CC-CV charging strategy of the proposed control, the secondary current and voltage measurements are required. The current and voltage control are made by a boost converter on the secondary side, as depicted in Figure 9.

In order to achieve the maximum efficiency in every stage of the charging process, the control has to adapt its parameters conveniently. For the next mathematical analysis, please consider that there are three resistances associated to the load, as shown in Figure 9. R_{Bat} models the battery with its internal resistance. This parameter can be defined from the voltage

and power requirements of the battery. R_{eq} represents the resistance at the input of the DC/DC converter. The DC/DC converter works as an impedance adapter so that R_{Bat} and R_{eq} are related as a function of the duty cycle D . Specifically, for the proposed DC/DC converter, the equivalent resistance (R_{eq}) can be defined as:

$$R_{eq} = (1 - D)^2 R_{Bat} \quad (1)$$

Finally, R_L is the resistance measured at the input of the rectifier. The rectification stages makes that:

$$R_L = \frac{8(1 - D)^2}{\pi^2} R_{Bat} \quad (2)$$

According to the equation in Table 5, the theoretical efficiency η_{th} is:

$$\eta_{th} = \frac{\frac{8(1-D)^2}{\pi^2} R_{Bat}}{R_1 \left(R_2 + \frac{8(1-D)^2}{\pi^2} R_{Bat} \right)^2 + R_2 + \frac{8(1-D)^2}{\pi^2} R_{Bat}} \quad (3)$$

It can be observed that the theoretical efficiency depends directly on the duty cycle of the DC/DC converter. Thus, there is an optimum D value to achieve maximum efficiency. However, tuning the duty cycle also changes the output battery. In order to maintain constant this voltage, the input voltage must vary accordingly. In particular, the voltage at the battery (V_{Bat}) is:

$$V_{Bat} = \frac{16\sqrt{2}R_{Bat}V_1\omega M(1 - D)}{R_1R_2\pi^3 + \pi R_18(1 - D)^2R_{Bat} + \pi^3\omega^2M^2} \quad (4)$$

As expected, the output voltage also depends directly on the duty cycle of the DC/DC converter and on the input voltage of the system. In order to control the output voltage, several combinations can be selected. For our MEPT implementation, a simple but effective approach will be followed. First, the controller on the secondary side sets the duty cycle which leads to the maximum efficiency. Then, it detects which input voltage is required to get the expected voltage at the battery. To determine the optimal D and V_1 , the controller looks up in an internal table stored in the local memory. For each battery resistance R_{Bat} , the table stores the correct values for D and V_1 . As the relative position between the coils do not change, these two parameters are constant for the same R_{Bat} . Thus, we can make use of a recorded table to identify the optimal configuration of the power converters. This table is completed with an experimental evaluation in a phase previous to the installation of the charger. With the pre-stored table, the controller is simplified into the following main steps. First, the equivalent resistance of the battery is estimated from measurements V_m and I_m . With this value, the control looks up at the pre-stored table to identify the optimal D and V_1 . Since the control is on the secondary side, it can directly adjust D . Finally, the controller communicates with the primary side to inform about the input voltage it must set.

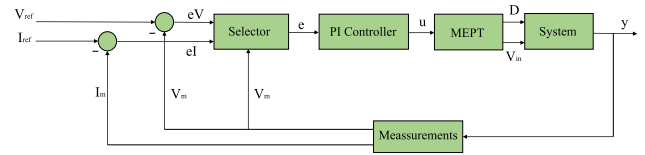


FIGURE 12. Control scheme for CC-CV charging.

Detecting foreign objects is indispensable for EV wireless chargers. When an object appears between the primary and secondary coils, the electrical parameters of the coils change. These changes may affect the charging process degrading the power transfer or even provoking some hazards due to the heating of the foreign object. Considering the gap, foreign objects such as coins, a piece of aluminium sheet or a nail may be accidentally placed in the area between the two coils. Algorithms for Foreign Object Detection (FOD) could contribute to a safer charge. These algorithms can be classified in three broad groups [27]: sensor-based detection, measuring parameter variations and sensing pattern based. Sensor-based variations can be implemented with several detection gadgets such as temperature sensors, pressure sensors or image cameras. Their main advantages are high sensitivity and the ability of detecting metal objects. On the other hand, implementing this kind of detection systems can be expensive, being their use impossible for some applications like light weight vehicles wireless chargers. Alternatively, measuring parameters variations is a cheaper solution to detect foreign objects. Parameters like self-inductance, quality factor or currents can be used. This method is limited by misalignment and it can be only used for low power applications. Finally, sensing pattern based presents high accuracy and sensitivity being independent from misalignment or the environment. This method uses an auxiliary coil to detect the object. Its limitations include non detecting small ferromagnetic objects. Considering the design premises of our e-scooter, measuring the electrical parameters outstands as the most convenient option for FOD.

This type of FOD technique is based on the fact that when a metal object is placed between the primary and the secondary coils, the self-inductances and mutual inductance of the coils decrease their values [28]. On the other hand the resistance of the coils increase their value. Some simulations have been released in order to study the effect of these changes on our designed wireless charger. For a simplicity purpose, we assume that all the inductances are diminished by factor β_L and the resistances are increased by factor β_R . Figure 13 shows the voltage variations on the primary coil. Based on these values, a FOD control may be included on the primary so when relevant changes on the voltage of the primary coil (V_L) are detected, the charging process is interrupted. Additional parameters should be checked to verify that the wireless charger is operating correctly. For instance, a current sensor may be installed on the primary side to detect short circuits on the secondary side. Under this condition, the current on the primary side increases and it is necessary to disconnect the primary coil.

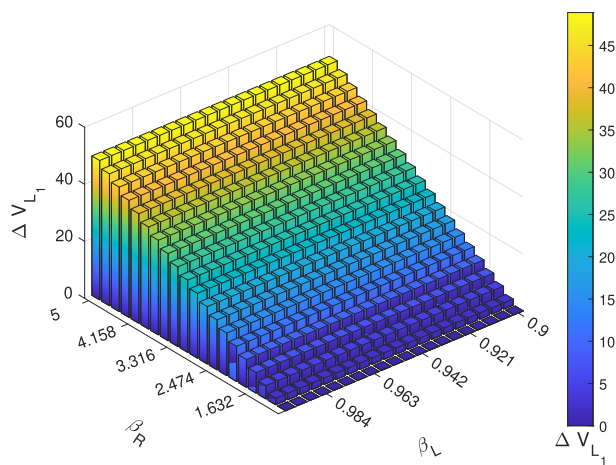


FIGURE 13. Voltage variations on the primary coil.

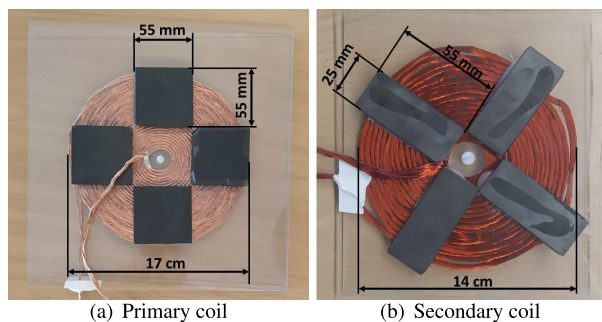


FIGURE 14. Implemented coils.

V. EXPERIMENTAL RESULTS

In order to validate the simulated results, a prototype has been implemented in the laboratory. The prototype is tested with an e-scooter model OutSider E-Evolution 8,5 Phoenix at 100 W. According to the SAE J2954 standard, the operating frequency is established at 85 kHz, which is the frequency provided by the primary inverter. Short-circuits have been avoided in the full bridge inverter by using PWM signals with a duty cycle lower than 50%. By using a duty cycle close to 50%, we ensure that short-circuits do not appear. This can be achieved in the programming stage, where this restriction can be programmed in the microcontroller. Losses are not relevant with this type of configuration [29].

Both coils have been made following the design of Section II. The implementation of both coils (primary and secondary) can be seen in Figure 14. The coils include ferrite tiles in the optimal layout as analysed in a previous Section.

The electrical parameters of the coils are measured with a Rohde & Schwarz HM8118 LCR meter. The real values of inductance are compared with the simulated values. The measured values are 63.148 μH for the primary coil and 24.749 μH for the secondary coil. These values are very close to the simulations, which validates the design process followed in this work. Table 7 shows a comparison of the simulated values and the measured ones.

The values of the capacitors are calculated using the expressions presented in Table 4 for a SS compensation topology. The theoretical compensation capacitors for 85 kHz were

TABLE 7. Comparison of simulated and measured values for the coils.

Parameter	Simulated	Measured
$L_1(\mu\text{H})$	63.5747	63.148
$L_2(\mu\text{H})$	24.6846	24.749
$M(\mu\text{H})$	7.8145	6.314

TABLE 8. Compensation capacitors value.

Parameter	Theoretical value	Measured
$C_1(\text{nF})$	55.52	55.78
$C_2(\text{nF})$	142.03	143.84

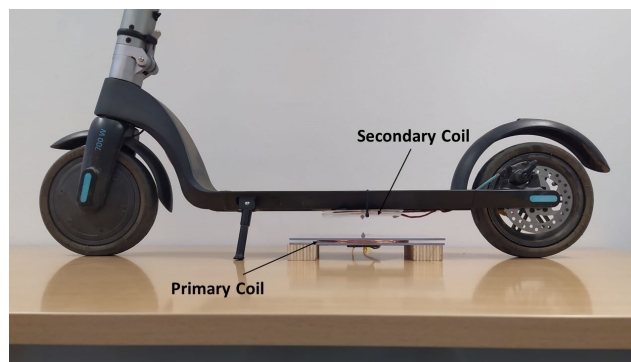


FIGURE 15. Designed coils on real e-scooter.

TABLE 9. Electrical measurements of the e-scooter wireless charger.

Parameter	Value
V_1	12.3 V
V_2	41.2 V
I_1	13.9 A
I_2	3.17
V_{DC}	38.5 V
Power	100.1 W
Efficiency	94.69 %

55.52 nF for the primary side and 142.03 nF for the secondary side. The final values of the compensations capacitors can be seen in Table 8. Minor differences are due to the tolerance of the components.

The final configuration of the coils on the scooter is presented in Figure 15. The receiver coil perfectly fits in the e-scooter base. In order to operate with the design gap, the primary coil is elevated some centimeters from the ground. The scooter stand helps this design requirement to be fulfilled without any additional structure.

In order to achieve the target charging power, in this experiment the input DC voltage to the charger is set to 15.12 V, leading to the voltage and current at the AC primary and secondary sides in Figure 16 and 17 respectively. Specifically, the electrical parameters are measured at the primary inverter output and at the secondary rectifier input, referred to V_1 , I_1 , V_2 and I_2 as indicated in Figure 10.(a). The measurements can be seen in Table 9. The results show an efficiency of 94.69 % in the AC power transfer.

The proposed CC-CV control has also been implemented in an Arduino Mega board. A digital output pin has been used

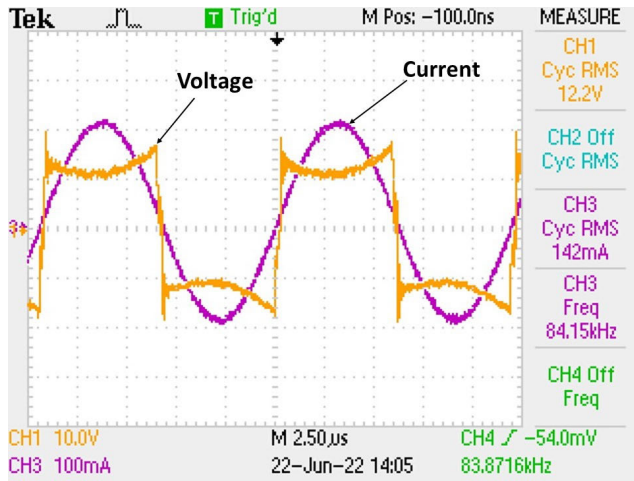


FIGURE 16. Voltage and current on the primary side.

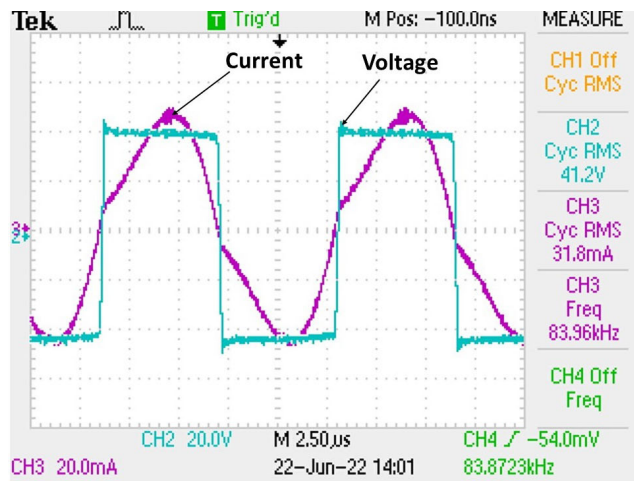


FIGURE 17. Voltage and current on the secondary side.

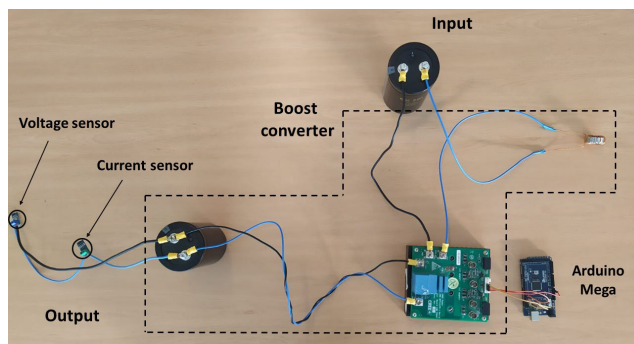


FIGURE 18. DC/DC converter, sensors and controller.

for the PWM signal, which regulates the duty cycle D in the boost converter. Two analog input pins are used to read I_m and V_m . With these two measurements, the algorithm control shown in Figure 12 will be executed in order to adjust the charging process. The converter used for the implementation can be seen in Figure 18. In this implementation V_{ref} and I_{ref} were constant to 40 V and 2.5 A respectively. Figure 19 shows the charging process depending on the equivalent resistance of the battery. It can be observed the two charging phases, as expected.

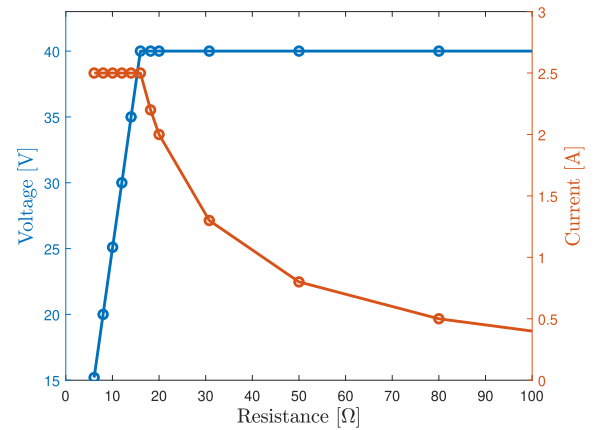


FIGURE 19. CC-CV charging implementation.

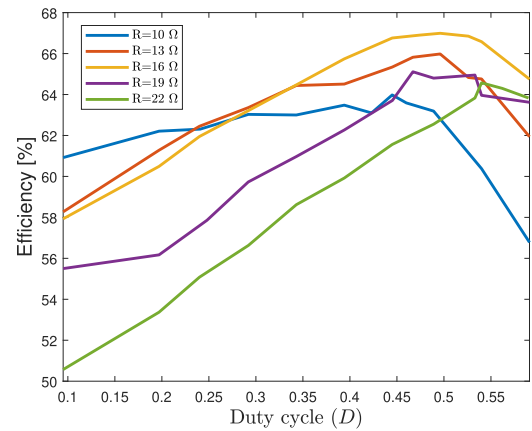


FIGURE 20. System efficiency for different duty cycles and equivalent resistance.

The efficiency of this converter has been studied in order to check the performance of the system. The efficiency of the converter is mostly above 90% for several equivalent resistances. As for the complete system, the AC/AC efficiency (measured at the output of the primary inverter and the input of the secondary rectifier) is 94.69%. However, the DC/DC efficiency (measuring at the input of the inverter and at the battery terminals) was in the range from 62% to 67%. The exact quantity depends of the equivalent resistance value of the load as can be seen in Figure 20. In this Figure, the variations of the efficiency with the duty cycle can be seen. When compared with wireless chargers for cars, this value is low. This is due to the low power levels that we are considering in this application. For the managed power, the effects of the non-idealities of the components are more relevant, so the parasitic resistances of the transistors and diodes notably degrade the system efficiency. The same effects were perceived in the low-power application described in [30].

For the implementation of the MEPT control, these experimental results are used to complete the internal value that the controller looks up to set the values of D and V_1 in order to maximize the efficiency while keeping the voltage constant at the battery input. These parameters depend on the equivalent resistance of the battery, which is estimated previously to derive the appropriate configuration setting. As misalignment

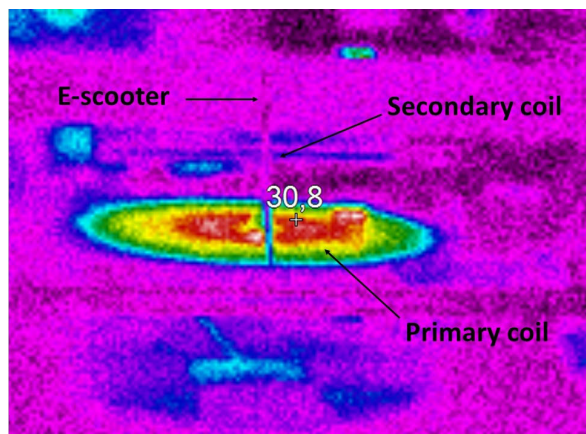


FIGURE 21. Thermal effects on e-scooter.

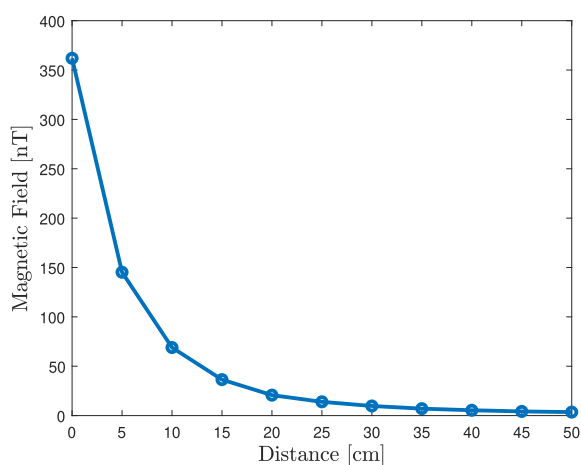


FIGURE 22. Magnetic field measurement at different positions from the center of the primary coil.

conditions are not expected in our application, these data are simple to store and to look-up.

As a valuable feature about the practicability of the wireless charger, thermal effects have been evaluated. The temperature reached by the charger when the process has taken 30 minutes can be seen in Figure 21. It shows that wireless charging does not affect the temperature in the e-scooter, which makes the charging system feasible for its use even when an immediate drive will take place. These effects of the charging on the secondary side have been achieved thanks to the design, which tries to minimize the current on the secondary coil. The charger element that reaches the highest temperature is the primary coil, with a maximum value of 31 °C. This does not constitute a significant limitation as the primary coil is expected to be embedded.

In order to satisfy the ICNIRP exposure limits, the magnetic field around the coils was measured and its variation with distance can be seen in Figure 22. The Gauss meter SPECTRAN NF-5030 is used to measure EMI under different distances away from the primary coil's center. The magnetic field strength is far below 27 μT , which demonstrates the compliance of the proposed design with safety and EMI restrictions for humans.

VI. CONCLUSION

E-scooters are becoming an essential way of transportation in our cities. For this reason, advanced techniques to ease their charging are needed. In this article, we designed and developed a magnetic resonant charger for a commercial e-scooter. The design of the coils was made using Ansys Maxwell software considering the effect of the vehicle on the WPT charging. Important features such as the layout of the ferrite tiles and the coil dimensions are addressed to achieve an optimal solution that aims to get a high efficiency and low costs. The selection of the compensation topology was also carried out, showing that SS compensation is the most suitable for this application. We have also included a feasible CC-CV control to guarantee that the charger is compatible with most common e-scooters, even when their batteries have different voltage levels. The application of all these design features in one real e-scooter has not been reported in the related literature. The results obtained from a real implementation showed an efficiency of 94.69% in the AC transmission, no relevant thermal effects on the e-scooter and compliance with the magnetic field restrictions.

Future works will be focused on the effective use of power electronics for a platform with several wireless chargers as well as the design of an optimal multi-coil system.

REFERENCES

- [1] Sources of Greenhouse Gas Emissions | U.S. EPA. Accessed: Feb. 1. [Online]. Available: <https://www.epa.gov/ghgemissions/sources-greenhouse-gas-emissions>
- [2] O. Altıntasi and S. Yalcinkaya, "Siting charging stations and identifying safe and convenient routes for environmentally sustainable E-scooter systems," *Sustain. Cities Soc.*, vol. 84, Sep. 2022, Art. no. 104020.
- [3] Y. Wang, J. Wu, K. Chen, and P. Liu, "Are shared electric scooters energy efficient?" *Commun. Transp. Res.*, vol. 1, Dec. 2021, Art. no. 100022.
- [4] A. Li, P. Zhao, X. Liu, A. Mansourian, K. W. Axhausen, and X. Qu, "Comprehensive comparison of E-scooter sharing mobility: Evidence from 30 European cities," *Transp. Res. D, Transp. Environ.*, vol. 105, Apr. 2022, Art. no. 103229.
- [5] M. S. Kumar and S. T. Revankar, "Development scheme and key technology of an electric vehicle: An overview," *Renew. Sustain. Energy Rev.*, vol. 70, pp. 1266–1285, Apr. 2017.
- [6] S. Statharas, Y. Moysoglou, P. Siskos, G. Zazias, and P. Capros, "Factors influencing electric vehicle penetration in the EU by 2030: A model-based policy assessment," *Energies*, vol. 12, no. 14, p. 2739, Jul. 2019.
- [7] *Examining the Impact of a Sustainable Electric Micromobility Approach in Europe*. EIT Innoenergy. Accessed: Feb. 1. [Online]. Available: <https://www.innoenergy.com/discover-innovative-solutions/reports/micromobility-report/>
- [8] S. I. Kwag, U. Hur, and Y. D. Ko, "Sustainable electric personal mobility: The design of a wireless charging infrastructure for urban tourism," *Sustainability*, vol. 13, no. 3, p. 1270, Jan. 2021.
- [9] Z. Yan, Y. Zhang, K. Zhang, B. Song, S. Li, T. Kan, and C. C. Mi, "Fault-tolerant wireless power transfer system with a dual-coupled LCC-S topology," *IEEE Trans. Veh. Technol.*, vol. 68, no. 12, pp. 11838–11846, Dec. 2019.
- [10] A. Triviño, J. M. González-González, and J. A. Aguado, "Wireless power transfer technologies applied to electric vehicles: A review," *Energies*, vol. 14, no. 6, p. 1547, Mar. 2021.
- [11] SAE International, *Wireless Power Transfer for Light-Duty Plug-in Electric Vehicles and Alignment Methodology*, SAE, Standard TIR J2954, 2020.
- [12] H. Hayashi, T. Sasatani, Y. Narusue, and Y. Kawahara, "Design of wireless power transfer systems for personal mobility devices in city spaces," in *Proc. IEEE 90th Veh. Technol. Conf. (VTC-Fall)*, Sep. 2019, pp. 1–5.
- [13] C. H. Kwan, J. M. Arteaga, N. Pucci, D. C. Yates, and P. D. Mitcheson, "A 110W E-scooter wireless charger operating at 6.78 MHz with ferrite shielding," in *Proc. IEEE PELS Workshop Emerg. Technol., Wireless Power Transf. (WoW)*, Jun. 2021, pp. 1–4.

- [14] P. K. Joseph, D. Elangovan, and P. Sanjeevikumar, "System architecture, design, and optimization of a flexible wireless charger for renewable energy-powered electric bicycles," *IEEE Syst. J.*, vol. 15, no. 2, pp. 2696–2707, Jun. 2021.
- [15] V. Kindl, R. Pechanek, M. Zavrel, T. Kavalir, and P. Turjanica, "Inductive coupling system for electric scooter wireless charging: Electromagnetic design and thermal analysis," *Electr. Eng.*, vol. 102, no. 1, pp. 3–12, Mar. 2020.
- [16] E. S. Lee, "Frequency-modulation-based IPT with magnetic communication for EV wireless charging," *IEEE Trans. Ind. Electron.*, vol. 70, no. 2, pp. 1398–1408, Feb. 2023.
- [17] A. Triviño-Cabrera, J. M. Gonzalez-Gonzalez, and J. A. Aguado, "Design and implementation of a cost-effective wireless charger for an electric bicycle," *IEEE Access*, vol. 9, pp. 85277–85288, 2021.
- [18] *Ansys Maxwell | Electromechanical Device Analysis Software*, Ansys, Canonsburg, PA, USA, 2023.
- [19] *Knot | Dock, Lock and Charge Your Scooters*. Accessed: Feb. 1. [Online]. Available: <https://www.knotcity.com/en/>
- [20] V.-B. Vu, A. Ramezani, A. Trivino, J. M. Gonzalez-Gonzalez, N. B. Kadandani, M. Dahidah, V. Pickert, M. Narimani, and J. Aguado, "Operation of inductive charging systems under misalignment conditions: A review for electric vehicles," *IEEE Trans. Transp. Electrific.*, vol. 9, no. 1, pp. 1857–1887, Mar. 2023.
- [21] A. Triviño-Cabrera, J. M. González-González, and J. A. Aguado, *Wireless Power Transfer for Electric Vehicles: Foundations and Design Approach*. Springer, 2020.
- [22] V. Shevchenko, O. Husev, B. Pakhaliuk, O. Karlov, and I. Kondratenko, "Coil design for wireless power transfer with series-parallel compensation," in *Proc. IEEE 2nd Ukraine Conf. Electr. Comput. Eng. (UKRCON)*, Jul. 2019, pp. 401–407.
- [23] A. Delgado-Expósito, "Analysis and guidelines for inductive power transfer links design," Ph.D. thesis, Automática, Ingeniería Electrónica e Informática Ind., E.T.S.I. Ind. (UPM), Madrid, Spain, 2021.
- [24] Y. J. Hwang and J. Y. Jang, "Design and analysis of a novel magnetic coupler of an in-wheel wireless power transfer system for electric vehicles," *Energies*, vol. 13, no. 2, p. 332, Jan. 2020.
- [25] M. Budhia, G. A. Covic, and J. T. Boys, "Design and optimization of circular magnetic structures for lumped inductive power transfer systems," *IEEE Trans. Power Electron.*, vol. 26, no. 11, pp. 3096–3108, Nov. 2011.
- [26] C. Ziegler, S. Weber, G. Heiland, and D. Kraus, "Influences of WPT-coil losses and coupling coefficient on the resonance circuits of wireless power transfer systems," in *Proc. PCIM Eur.; Int. Exhib. Conf. Power Electron., Intell. Motion, Renew. Energy Energy Manag.*, May 2017, pp. 1–7.
- [27] J. Lu, G. Zhu, and C. C. Mi, "Foreign object detection in wireless power transfer systems," *IEEE Trans. Ind. Appl.*, vol. 58, no. 1, pp. 1340–1354, Jan. 2022.
- [28] J. Kim, J. Kim, S. Kong, H. Kim, I.-S. Suh, N. P. Suh, D.-H. Cho, J. Kim, and S. Ahn, "Coil design and shielding methods for a magnetic resonant wireless power transfer system," *Proc. IEEE*, vol. 101, no. 6, pp. 1332–1342, Jun. 2013.
- [29] J. M. Gonzalez-Gonzalez, A. Trivino-Cabrera, and J. A. Aguado, "Assessment of the power losses in a SAE J2954-compliant wireless charger," *IEEE Access*, vol. 10, pp. 54474–54483, 2022.
- [30] A. Trivino, J. Sanchez, and A. Delgado, "Efficient methodology of the coil design for a dynamic wireless charger," *IEEE Access*, vol. 10, pp. 83368–83378, 2022.



ALICIA TRIVIÑO-CABRERA received the master's degree in telecommunication engineering and in computer science engineering from the University of Málaga, Spain, in 2002 and 2008, respectively.

Her thesis, which she defended, in 2007, focused on wireless networks. She currently holds a position as Associate Professor with the University of Málaga. Since 2011, her research interest includes wireless power transfer. In the field of electric vehicle wireless chargers, she has played an active role in designing and developing several prototypes, including features such as bi-directionality and dynamic charging.



JUAN C. QUIRÓS was born in Estepona, Spain. He received the B.Sc. degree in electrical engineering from the University of Málaga, Spain, in 2021, where he is currently pursuing the master's degree in mechatronic engineering. He received the Best Student of the Year Award for his B.Sc. degree.



JOSE M. GONZÁLEZ-GONZÁLEZ was born in Málaga, Spain. He received the master's degree in industrial engineering from the University of Málaga, Spain, in 2015, and the Ph.D. degree in electrical engineering, in 2021. His thesis focused on the design of a prototype with bi-directional features. He also has practical experience working on smart grids and renewable energy projects, with some publications on the integration of battery energy storage.



JOSÉ A. AGUADO (Member, IEEE) was born in Málaga, Spain. He received the degree in electrical engineering and the Ph.D. degree from the University of Málaga, Málaga, in 1997 and 2001, respectively.

He is currently a Full Professor and the Head of the Electrical Engineering Department, University of Málaga. He has led more than 40 publicly funded research and consulting projects on the operation and planning of smart grids and wireless power transfer.

...